Internal Tides Drive Nutrient Fluxes Into the Deep Chlorophyll Maximum Over Mid-ocean Ridges

Robyn E. Tuerena[1,2], Richard G. Williams[1], Claire Mahaffey[1], Clément Vic[3], J. A. Mattias Green[4], Alberto Naveira-Garabato[3], Alexander Forryan[3], and Jonathan Sharples[1]

[1]School of Environmental Sciences, University of Liverpool, Liverpool, UK, [2]School of GeoSciences, University of Edinburgh, Edinburgh, UK, [3]School of Ocean and Earth Sciences, University of Southampton, Southampton, UK, [4]School of Ocean Sciences, Bangor University, Bangor, UK

Abstract Diapycnal mixing of nutrients from the thermocline to the surface sunlit ocean is thought to be relatively weak in the world's subtropical gyres as energy inputs from winds are generally low. The interaction of internal tides with rough topography enhances diapycnal mixing, yet the role of tidally induced diapycnal mixing in sustaining nutrient supply to the surface subtropical ocean remains relatively unexplored. During a field campaign in the North Atlantic subtropical gyre, we tested whether tidal interactions with topography enhance diapycnal nitrate fluxes in the upper ocean. We measured an order of magnitude increase in diapycnal nitrate fluxes to the deep chlorophyll maximum (DCM) over the Mid-Atlantic Ridge compared to the adjacent deep ocean. Internal tides drive this enhancement, with diapycnal nitrate supply to the DCM increasing by a factor of 8 between neap and spring tides. Using a global tidal dissipation database, we find that this spring-neap enhancement in diapycnal nitrate fluxes is widespread over ridges and seamounts. Mid-ocean ridges therefore play an important role in sustaining the nutrient supply to the DCM, and these findings may have important implications in a warming global ocean.

Plain Language Summary The subtropical gyres cover an extensive area of the global ocean and account for ~30% of carbon export to the deep ocean. The pattern of the winds induces downwelling in these gyres and leads to surface waters being relatively nutrient impoverished. Biological production in the subtropical gyres is primarily limited by the availability of nitrate, which can be increased through mixing in the underlying thermocline. Internal tides can enhance mixing in the ocean interior close to steep sloping topography; deep in the ocean interior, this mixing is a key component of ocean physics. In our field study, we reveal the mixing extending up toward the surface and measured a tenfold increase in nitrate fluxes to phytoplankton in the surface ocean over the Mid-Atlantic Ridge compared to in the surface waters in the adjacent deeper ocean. Importantly, nitrate fluxes over the ridge varied fortnightly with an eightfold increase from neap to spring tides. These inferences of enhanced mixing and nutrient supply along ridges and seamounts are relevant for the rest of the global ocean given the ubiquitous nature of the tides.

1. Introduction

Internal tides are viewed as a major energy source for upper-ocean mixing (Kunze, 2017; Waterhouse et al., 2014). The resulting diapycnal nutrient fluxes driven by this upper-ocean mixing are widely recognized as being important in sustaining primary productivity in the continental shelf seas (Rippeth & Inall, 2002; Sharples et al., 2007; Tweddle et al., 2013; Villamaña et al., 2017). In contrast, these diapycnally driven nutrient fluxes are viewed as relatively unimportant in the open ocean. In the deep open ocean, diapycnal mixing is spatially patchy, the turbulent kinetic energy dissipation varying by 1 to 2 orders of magnitude, and with enhanced mixing extending up to 1–2 km above rough topography (Kunze et al., 2006; Polzin et al., 1997; Waterhouse et al., 2014). This enhanced mixing is associated with the breaking of internal waves driven by the interaction of the internal tide and rough topography (Egbert & Ray, 2000; Garrett & Kunze, 2007; Munk & Wunsch, 1998). In the upper open ocean, diapycnal mixing is sustained by internal tides (Hibiya & Nagasawa, 2004; Kunze, 2017; Lavergne et al., 2019; Lefauve et al., 2015; Melet et al., 2016) and also the near-inertial inputs of wind energy (Alford et al., 2012; Whalen et al., 2018). The low inputs of wind energy into the subtropical gyres, particularly in summer months, have led to a prevailing view that the diapycnal
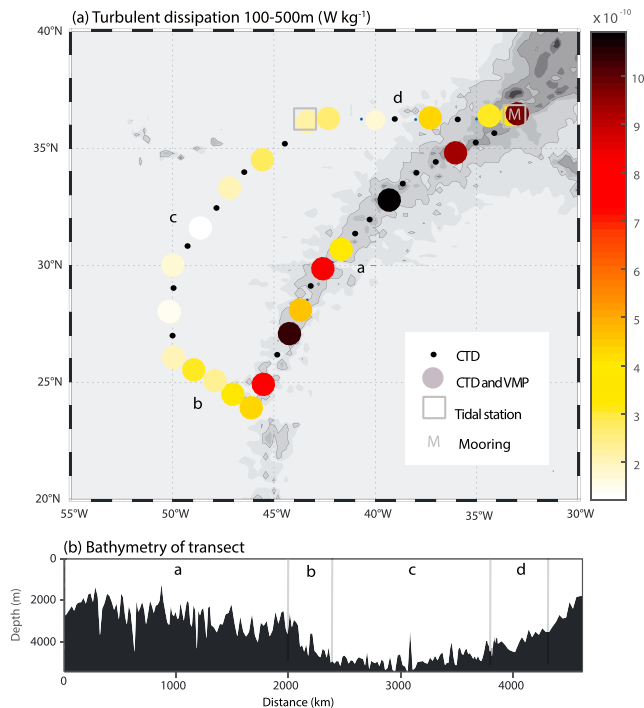
Figure 1. (a) Map of study area displaying locations of full water column CTD (conductivity, temperature, depth) and Vertical Microstructure Profiler sampling over the Mid-Atlantic Ridge and in the adjacent abyssal ocean. Filled circles indicate the average water column turbulent kinetic energy dissipation between 100 and 500 m, which are enhanced along the ridge (eastern transect). The on- and off-ridge tidal stations and mooring are highlighted in the northern transect. (b) The changing bathymetry plotted against distance along the cruise track, the on-ridge, a; off-ridge, d; and cross ridge, b, d, sections are highlighted. VMP = Vertical Microstructure Profiler.

nutrient flux to the surface ocean is relatively weak. In this study, we explore the relative importance of the internal tide in providing an enhancement in the diapycnal supply of nutrients in the upper open ocean along topographic ridges and regions of shallow bathymetry.

The diapycnal flux of a nutrient (N_u) is the product of the vertical gradient of the tracer concentration ($\partial N_u/\partial z$) and the local diapycnal diffusivity (K_z), that is, nutrient flux $= -K_z (\partial N_u/\partial z)$. The diapycnal diffusivity is estimated from the local rate of dissipation of turbulent kinetic energy and the inverse of buoyancy frequency (Osborn, 1980). Variability in K_z over the open ocean is revealed by microstructure measurements and typically ranges from $\sim 10^{-6}$ to 10^{-5} m^2/s in deep ocean basins and up to 10^{-4} to 10^{-2} m^2/s near ocean ridges and seamounts (Polzin et al., 1997; Waterhouse et al., 2014).

To affect nutrient fluxes and primary production, enhanced K_z from tidal energy must reach the base of the euphotic zone, where sharp nutrient gradients separate the dark nutrient-rich interior and the nutrient-deplete euphotic zone (Lewis et al., 1986, Sarmiento et al., 2004, Pelegri et al., 2006; Figure S1 in the supporting information). If either K_z or the nutrient gradient is increased, then the supply of "new" nutrients mixed up from the ocean interior is enhanced. During summer in the subtropical ocean, nutrients become exhausted in the mixed layer and throughout the euphotic zone. As a result, a chlorophyll feature in the subtropical ocean, the deep chlorophyll maximum (DCM), emerges at the base of the euphotic zone, concomitant with the upper thermocline. Measurements from the subtropical North Pacific indicate that the DCM might be locally important, accounting for 34% of particulate nitrogen export (Letelier et al., 2004). Enhanced diapycnal mixing from the interaction of internal tides with mid-ocean ridges may increase export production by augmenting the nutrient supply to the DCM.

In this paper, we determine how the internal tide drives changes in the diapycnal nitrate flux to the base of the DCM. We first present the analysis of observations from a field campaign within the North Atlantic subtropical gyre, over and adjacent to the Mid-Atlantic Ridge (section 2), which are compared to regional wind and tide estimates (section 3). We then employ a tidal model of energy dissipation to illustrate the larger-scale implications of the observed signal of enhanced diapycnal nutrient fluxes over complex topography (section 4), and then discuss the wider implications of the study for subtropical gyres (section 5).

2. Field Survey

2.1. Field Measurements

This field study took place in the North Atlantic subtropical gyre between 24°N to 36°N, to assess the influence of the internal tides on diapycnal nutrient fluxes over the Mid-Atlantic Ridge and the adjacent abyssal ocean (Figure 1). The sampling campaign was conducted on the RRS *James Clark Ross* during May to June 2015. The survey began in the northwestern corner of the study area at spring tide and continued in a clockwise direction around the transect. Salinity, temperature, and depth were measured using a conductivity, temperature, depth (CTD) system (Seabird 911+) with salinity calibrated onboard with discrete samples using an Autosal 8400B salinometer (Guildline). Photosynthetically active radiation from the CTD was used to calculate the euphotic layer depth, which was defined as the depth where photosynthetically active radiation decreased to 1% of the surface value. The CTD fluorescence sensor was calibrated using a Turner Trilogy fluorometer with measurements conducted in the upper 300 m.

At all stations micromolar nutrient analysis was carried out using a four-channel (nitrate, nitrite, phosphate, and silicate) Bran and Luebbe AAIII segmented flow, colorimetric, autoanalyzer. Certified reference
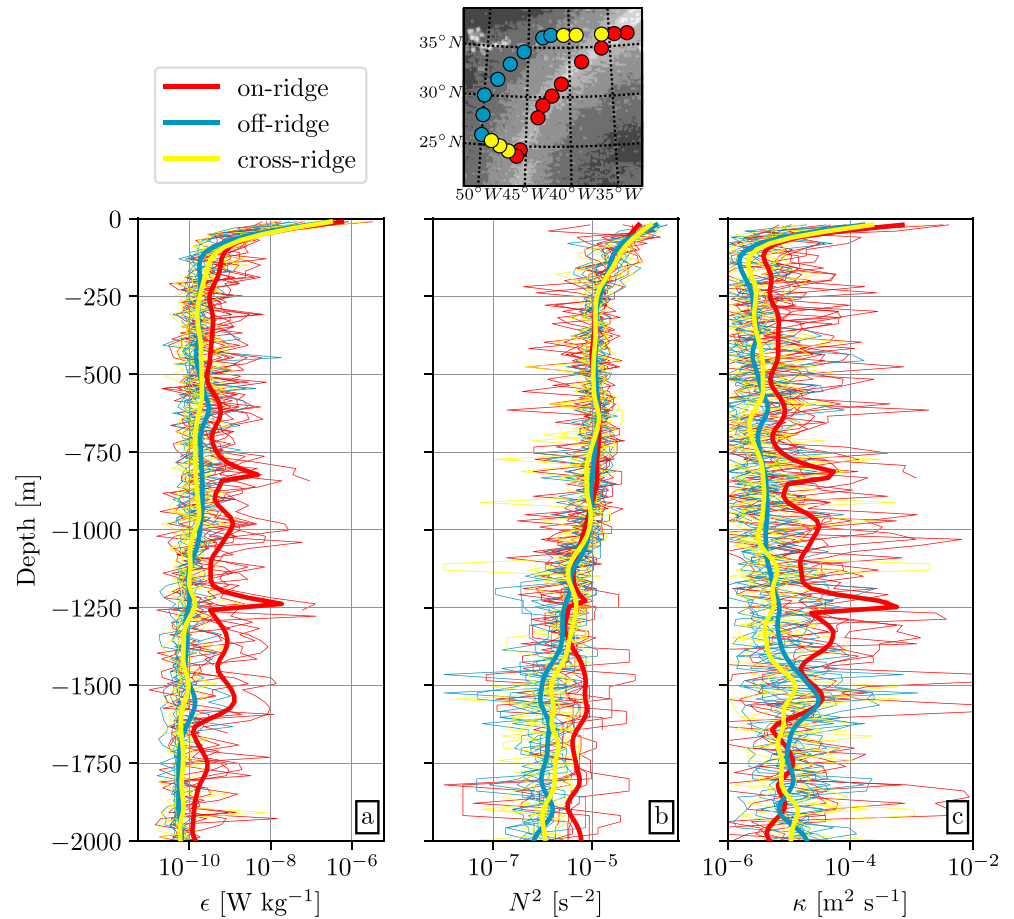
Figure 2. Depth profiles of (a) turbulent dissipation (W/Kg), (b) N^2 (s^{-2}), and (c) turbulent diffusivity (m^2/s) in the upper 2,000 m across our study site. Stations are defined as on ridge (red), cross ridge (yellow), and off ridge (blue).

materials (BU) were analyzed every two to three runs to ensure continued precision throughout the cruise, with cruise averages within the accepted range for each nutrient and a 99% precision. Two internal standards covering a wide range of concentrations for nitrate, phosphate, and silicate were analyzed in each run.

Full water column profiles of turbulent dissipation and diffusivity were made using a free falling Vertical Microstructure Profiler (VMP6000, Rockland Scientific). In addition to spatial coverage around the cruise track, the resolution of tidal semidiurnal variability was recorded by carrying out continuous profiling of the upper 1,000 m (sometimes down to 1,800 m) using a VMP2000 at two stations, one in the northeastern (on ridge) and one in the northwestern (off ridge) corner of the transect (Figure 1). At the on-ridge tidal station, continuous sampling for 25 and 15 hr was carried out during spring and neap tides, respectively, while at the off-ridge station continuous sampling was carried out for 20 hr during a spring tide. The microstructure for the temperature and velocity shear was measured on the length scales of dissipation of turbulent flows, typically a few millimeters to tens of centimeters. The rates of the dissipation of turbulent kinetic energy (ε (m^2/s^3)) were estimated following the methods by Oakey (1982).

Diapycnal diffusivity, K_z (m^2/s) was calculated from

$$K_z = \Gamma \frac{\varepsilon}{N^2} \ (m^2/s),\tag{1}$$

where N is the buoyancy frequency (s^{-1}) and Γ is the mixing efficiency (Figure 2). Based on the typical conditions measured in the upper 500 m during the cruise, Γ was taken to be constant at 0.2 (Gregg et al., 2018, and references therein).
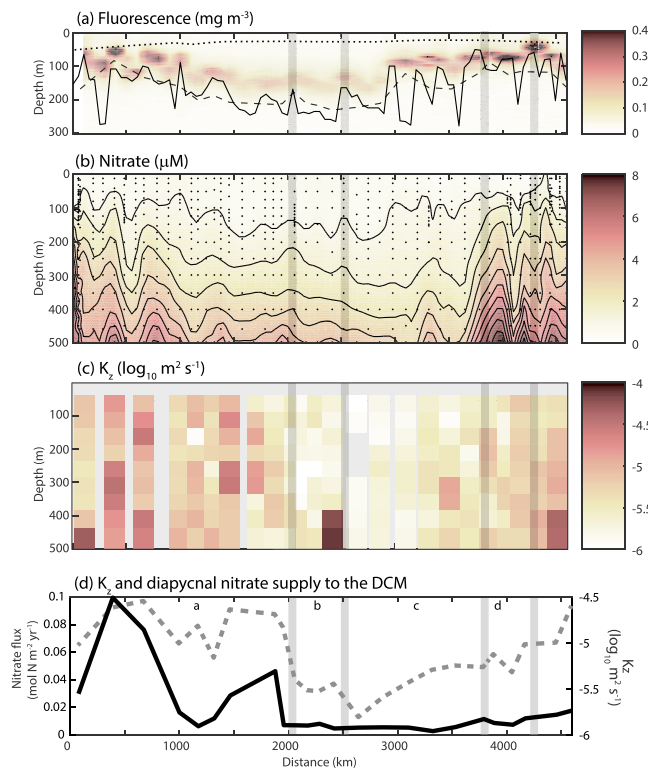
Figure 3. Along track changes in chlorophyll, nitrate, and K_z. (a) Fluorescence (mg/m^3) in the upper 300 m with the warmest colors indicating the DCM. The solid line shows the depth of the maximum nitrate gradient, the dashed line shows the depth at which chlorophyll decreases to 10% of its maximum, and the dotted line shows the depth of the mixed layer. (b) Nitrate concentrations (μM) in the upper 500 m against distance along cruise track. (c) Vertical diffusivity, K_z (log$_{10}$ m^2/s), in the upper 500 m as measured by the vertical microstructure profiler. (d) Mean diffusivity, K_z (dashed line) and estimated diapycnal nitrate supply to the DCM (solid line). Nitrate supply to the DCM was calculated from the convergence of the nitrate flux (nitrate gradient [mmol/m^4] multiplied by the diffusivity, K_z [m^2/s]), between the peak of the DCM and the depth at which chlorophyll drops to 10% the maximum chlorophyll concentration. Gray lines separate on-ridge, off-ridge, and cross-ridge sections labeled in Figure 1.

2.2. Enhanced Upper-Ocean Mixing Over the Mid-Atlantic Ridge

We designed a field experiment to test the hypothesis that the generation of internal tides over mid-ocean ridges and resulting internal wave breaking can drive increased diapycnal mixing and enhance nitrate fluxes to the base of the DCM. The field program provided estimates of diapycnal diffusivity K_z and nutrient fluxes over the Mid-Atlantic Ridge and adjacent abyssal ocean (Figure 1).

There is a consistent enhancement in the turbulent kinetic energy dissipation over the upper 2,000 m above the ridge relative to in the deeper basin (Figure 2a, blue versus red). Combining with the buoyancy frequency, there is then a systematic enhancement in the diapycnal mixing over the ridge by typically 1 order of magnitude over much of the water column (Figures 2b and 2c).

Now focusing on the upper 500 m, turbulent microstructure measurements revealed dissipation rates over the ridge that were enhanced by a factor of between 4 and 10 compared to off ridge (Figure 1a). The associated K_z is similarly enhanced, extending to the upper ocean and reaching the base of the DCM, where there was an increase from an average of 2.3×10^{-6} m^2/s in the basin to 1.3×10^{-5} m^2/s over the ridge (Figure 3a and Table 1). Spatial variability in K_z along the ridge section was partially due to the gradually deepening ridge crest toward the south (Figures 1 and 3) but was associated also with the spring-neap cycle and regions where the rough seafloor generates energetic high-mode internal waves that are prone to breaking and increasing K_z (Falahat et al., 2014; Vic et al., 2018).

Diapycnal nitrate fluxes to the DCM were determined by K_z combined with vertical nitrate gradients at the base of the DCM (Omand & Mahadevan, 2015; Sharples et al., 2007). There is a nitrate supply to the DCM whenever there is a convergence in the diapycnal nitrate flux. As nitrate becomes depleted above the DCM and the vertical nitrate gradient becomes small, then a diapycnal nitrate flux at the base of the DCM automatically corresponds to a diapycnal supply of nitrate. Enhanced diapycnal mixing increases the diapycnal nitrate flux at the base of the DCM and so increases the nitrate supply to the DCM, which can either increase nitrate in the DCM or possibly sustain more phytoplankton growth.

Table 1
Variation in Diapycnal Diffusivity and Diapycnal Nutrient Fluxes at the DCM Over Time and Space Scales

Diffusivity and diapycnal nitrate fluxes at the deep chlorophyll maximum		
(a) Diapycnal diffusivity (m^2/s)	On ridge	1.3×10^{-5} (0.5–1.8×10^{-5})
	Off ridge	2.3×10^{-6} (1.3–3.4×10^{-6})
	Spring (on ridge)	9.3×10^{-5} (2.2–16.4×10^{-5})
	Spring (off ridge)	4.6×10^{-6} (2.9–6.3×10^{-6})
	Neap (on ridge)	1.3×10^{-5} (1.0–1.6×10^{-5})
(b) Diapycnal nitrate supply (mol N·m^{-2}·year^{-1})	On ridge	0.030 (0.009–0.058)
	Off ridge	0.002 (0–0.005)
	Spring (on ridge)	0.271 (0.017–1.030)
	Spring (off ridge)	0.004 (0.002–0.007)
	Neap (on ridge)	0.032 (0.010–0.062)

Note. (a) The mean diffusivity at the base of the deep chlorophyll maximum (DCM; using a depth range between the depth of the DCM and the depth at which chlorophyll drops to 10% of the peak chlorophyll) from each profile was used to compute the zonally averaged diffusivity on and off ridge and the spring and neap variability at the tidal stations in Figure 1. (b) The estimates of diffusivity in (a) were combined with local nitrate gradients to calculate the diapycnal nitrate supply to the DCM (converted to mole of nitrogen per square meter per year). The ranges in parentheses represent 2σ. DCM = deep chlorophyll maximum.
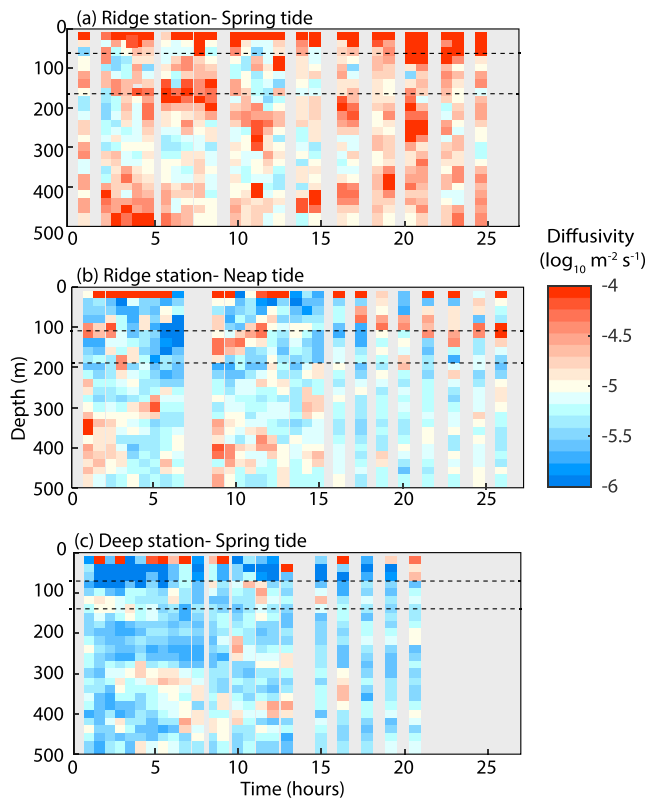
Figure 4. Tidal variation in vertical diffusivity at the on-ridge and off-ridge stations over 25-hr periods in the upper 500 m. (a) On-ridge station during the spring tide, (b) on-ridge station during the neap tide, and (c) off-ridge station during the spring tide ($\log_{10}$ m²/s). The dashed lines on each plot represent the depth interval used to calculate nutrient fluxes in Figure 5, from the DCM to where fluorescence decreases to 10% of its maximum.

There is an order of magnitude increase in the diapycnal nitrate flux between the off- and on-ridge sites (Figure 3d and Table 1). This ridge-enhanced diapycnal nitrate supply arises from both the increase in K_z and the increase in the vertical nitrate gradient on the ridge (Table 1). There are stronger vertical gradients at the base of the DCM over the ridge compared to off ridge for all macronutrients (N, P, and Si), further supporting the view of increased diapycnal mixing.

2.3. Internal Tides and Mixing Over Spring and Neap Cycles

The enhanced diapycnal mixing over the ridge compared to the abyssal ocean is likely to be generated by tidal interaction with rough topography (St Laurent & Garrett, 2002; Toole, 2007). In order to test this viewpoint, we conducted three time series stations with a turbulent microstructure profiler, each station covering one to two semidiurnal tidal cycles (Figure 4). Turbulent diffusivity in the base of the DCM on the ridge increased from 1.3×10^{-5} to 9.3×10^{-5} m²/s from neap to spring tides (Figures 4a and 4b) and was 3 times higher at neap tides and 20 times higher at spring tides than spring tide at the off-ridge site (Figures 4 and 5b). The enhanced tidal mixing and associated K_z on the ridge has a marked fortnightly spring-neap periodicity. This fortnightly variation in K_z produced by the barotropic tide flowing over rough topography has been discussed in previous field studies (Toole, 2007).

Observations of diapycnal diffusivity and vertical nitrate gradients over the ridge reveal an increase in diapycnal nitrate fluxes to the DCM from 0.03 to 0.27 mol N·m^{-2}·year^{-1} from neap to spring tides (Figures 5b–5d). The diapycnal nitrate flux becomes small in the surface mixed layer due to the depletion of mixed-layer nitrate. The diapycnal nitrate flux reaches a subsurface maximum at depths of around 100 m off the ridge and during the neap tide on the ridge but reaches a subsurface maximum at 60 m during the spring tide on the ridge. This depth structure of the diapycnal nitrate flux drives a supply of nitrate at depths between 50 and 100 m during the spring tide on the ridge and a loss of nitrate from depth between 100 and 150 m (Figure 5e, red line). There is a similar, but weaker in magnitude, structure for the nitrate supply associated with the neap tide on the ridge and the spring tide off the ridge (Figure 5e, yellow and blue lines). The variability in the diapycnal nitrate supply over a spring-neap cycle also alters the depth of the chlorophyll maximum, with the DCM shallowing from 100 to 50 m from neap to spring tides on the ridge, coinciding with the maximal nitrate supply (Figures 5e and 5f).

The on-ridge nitrate supply to the DCM at spring tide was 67 times higher than the off-ridge flux (Table 1). The strength of the diapycnic mixing on the ridge is related to both the spatial variability associated with seabed topography and the temporal variability driven by the spring-neap tidal cycle. In addition, nitrate fluxes over the ridge (Figure 3) vary according to changes in the vertical gradient in the nutrients and hotspots of expected mixing where there may be regions of supercritical seabed slope.

3. The Contribution of Tides and Winds to Diapycnal Nitrate Fluxes

During our summer survey, the surface mixed layer is relatively thin, only reaching depths of 20 to 50 m, and the layer of peak chlorophyll and the lower limb of the DCM lies within the seasonal pycnocline, at depths of 102 ± 35 and 165 ± 44 m, respectively. There are two primary candidates to drive the diapycnal mixing at the base of the DCM: wave breaking due to winds or tides.

To determine the impact of the winds relative to the tides over the relevant depth ranges, the kinetic energy content is evaluated at near-inertial and semidiurnal frequencies in the upper 500 m, which are taken to be representative of the dominant wind and M2 tidal frequencies, respectively. The time mean and standard deviation of the velocities were evaluated from mooring Acoustic Doppler current profiler (ADCP) data at
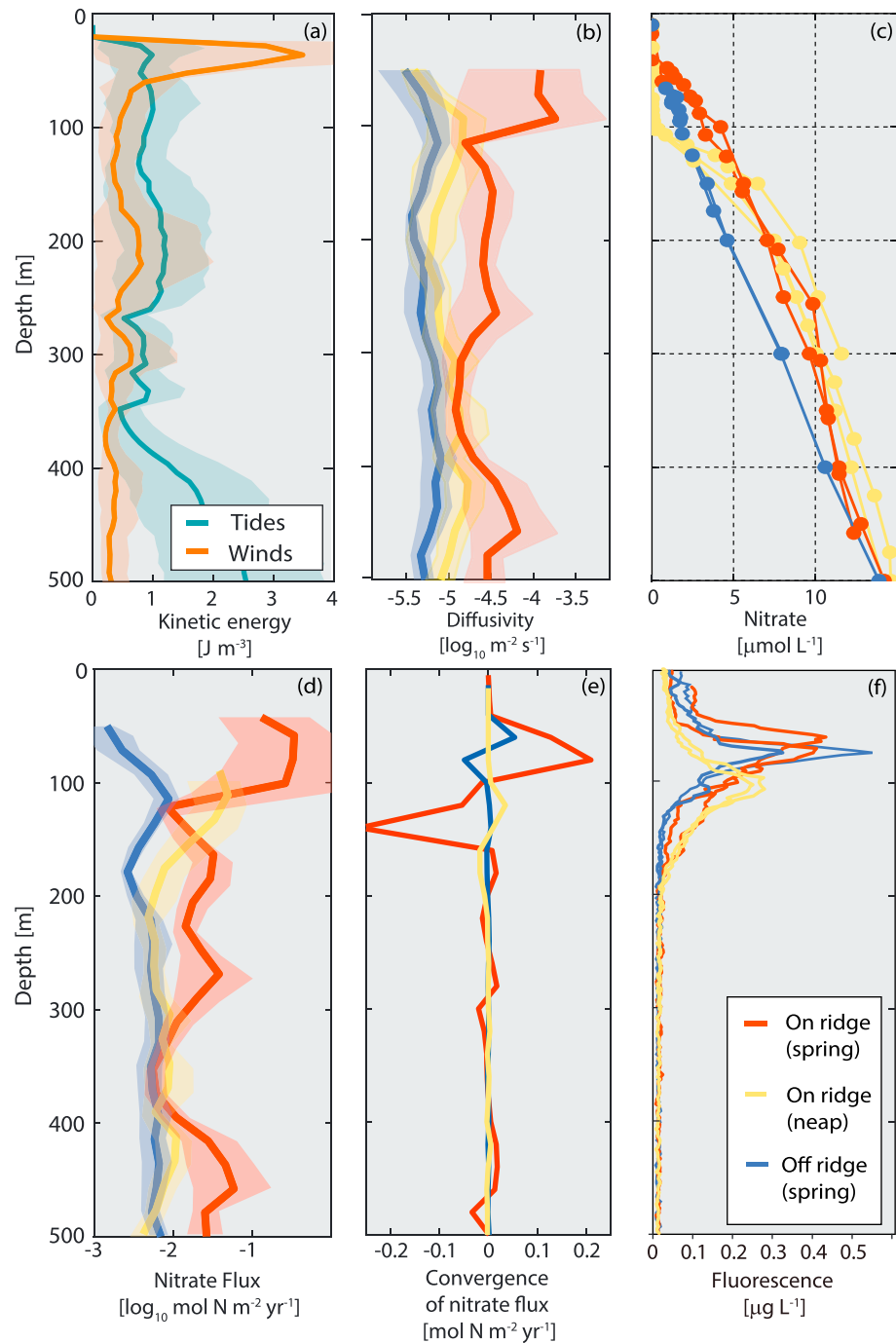
Figure 5. (a) Mean ($\pm 1\sigma$) profiles of kinetic energy per unit volume (J/m^3) for semidiurnal (blue) and near-inertial frequencies (orange), where semidiurnal signal is viewed as from the M2 tides and the near-inertial signal from the winds, computed from velocities from the Acoustic Doppler current profiler (ADCP) mooring (located at the on-ridge tidal sampling site). (b) Bootstrapped average and 95% confidence limits of diffusivity in the upper 500 m ($\log_{10} m^2/s$); (c) vertical nitrate profiles ($\mu mol/L$); (d) the implied diapycnal nitrate fluxes ($\log_{10}$ mol N·m^{-2}·year^{-1}) using the nitrate gradient (mmol/m^4); (e) local convergence of nitrate flux (mol N·m^{-2}·year^{-1}), positive indicates supply of nitrate, negative indicates loss of nitrate; and (f) fluorescence profiles from the conductivity, temperature, depth which were used to calculate the nitrate gradient (the depth range between the deep chlorophyll maximum and where the deep chlorophyll maximum decreases to 10% of its maximum).
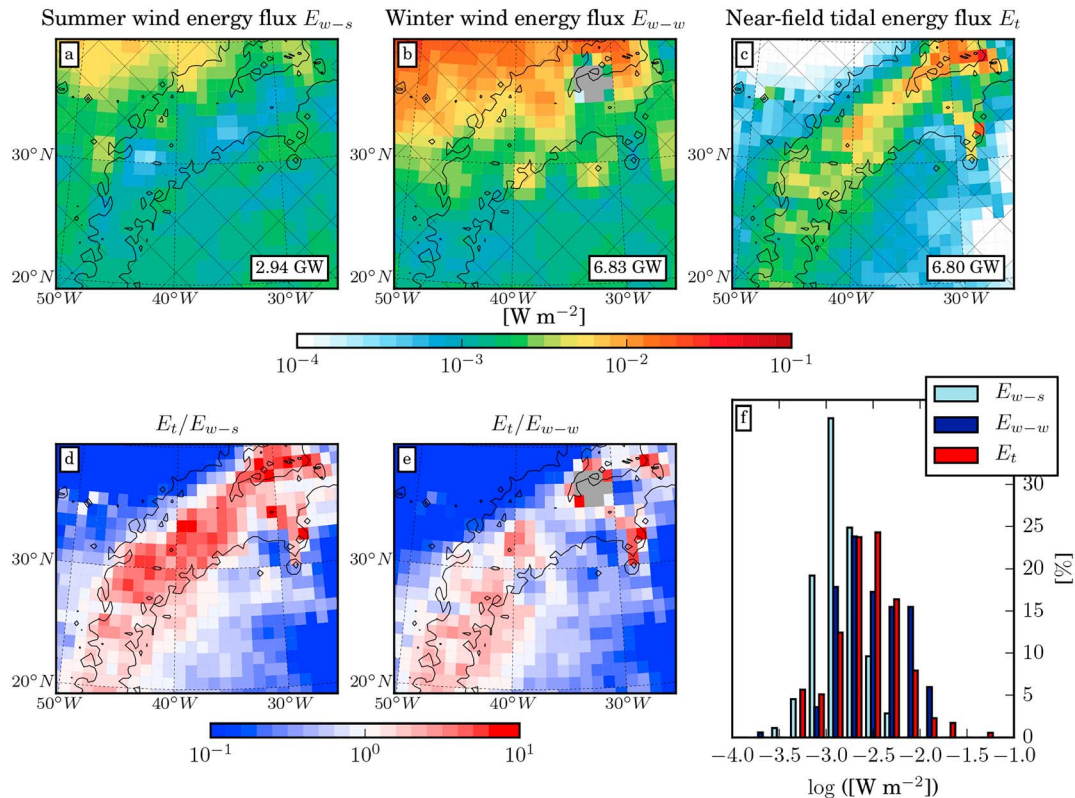
Figure 6. Regional estimates of near-field tidal and wind energy fluxes. (a) Winter wind energy flux, $E_{w\text{-}w}$, (b) summer wind energy flux, $E_{w\text{-}s}$, and (c) tidal energy flux, E_t (W/m²), including 2,000- and 4,000-m bathymetry (black contours), together with (d) ratio of the tidal energy flux/summer wind energy flux, (e) ratio of the tidal energy flux/winter wind energy flux, and (f) histogram of the three energy fluxes over the Mid-Atlantic Ridge, (hatch-free area in panels [a]—[c]), defined by latitude 20–38°N, longitude 25–50°W, and bathymetry <4,000 m. Integrated energy fluxes over the domain are given in panels (a)–(c) in gigawatt.

the on-ridge site (Figure 5a). Horizontal velocity fields were filtered at the M2 and inertial frequencies using a band-pass fourth-order Butterworth filter in the bandwidth $\left[\frac{\omega}{c}, c\omega\right]$ with $c = 1.25$ and $\omega = 1.4 \times 10^{-4}\,\text{s}^{-1}$ for the M2 frequency (Alford, 2003) and $\omega = 0.86 \times 10^{-4}\,\text{s}^{-1}$ for the inertial frequency. The kinetic energy per unit volume, $0.5\rho_0(u'^2 + v'^2)$, is evaluated from the filtered velocities u', v', and $\rho_0 = 1,025\,\text{kg/m}^{3}$. Note, however, that the near-inertial kinetic energy reservoir does not necessarily feed local turbulence. The wind contribution from the near-inertial energy input is mainly confined close to the surface in the upper 50 m, while the semidiurnal tidal energy input dominates over the wind energy input below the mixed layer, reaching a factor of 2 larger within the DCM (Figure 5d).

To provide an additional context, we compared the tidal and wind energy inputs over the Mid-Atlantic Ridge region (Figure 6). Specifically, we used the fraction of tidal energy conversion that goes into high-mode (>4) internal tides, E_t, from Vic et al. (2019). Vic et al. (2019) showed that this is an accurate estimate of the tidally driven "near-field" energy dissipation. Near field here refers to the fraction of the tidal energy input that dissipates into local turbulence (MacKinnon et al., 2017). E_t is enhanced over the ridge, where the tidal currents are stronger and the seafloor topography is rougher (Figure 6c; Vic et al., 2018); this locally generated tidal component is also referred to as the near-field dissipation (MacKinnon et al., 2017). The wind energy flux is the total wind energy input to near-inertial motions in summer ($E_{w\text{-}s}$) and in winter ($E_{w\text{-}w}$) from Whalen et al. (2018). The near-inertial motions lead to shear across the transition layer, and this process is a major component of mixing in the upper ocean (Alford et al., 2016).

The summer wind energy input is relatively modest due to light wind conditions but much stronger in winter, $E_{w\text{-}w}$, due to enhanced atmospheric storm activity (Figures 6a and 6b). The wind energy flux is enhanced in the northwestern corner of the area (Figures 6a and 6b), also coinciding with enhanced ocean mesoscale eddy activity (Whalen et al., 2018). Over the ridge, the tidal energy flux dominates the

wind energy flux in summer, with an input of 6.80 GW compared to 2.94 GW (Figures 6d and 6f, evaluated over hatch-free area). However, the tidal and wind energy fluxes become comparable in winter (Figures 6e and 6f), with a wind energy flux of 6.83 GW. Tidal- and wind-driven processes that lead to mixing are not totally independent. Tidal and near-inertial waves can interact nonlinearly and cascade down to dissipation (Cuypers et al., 2017). Nonetheless, at the time of the measurements, light-wind conditions did not favor those interactions.

In conclusion, the diapycnal mixing driving nutrient fluxes for the DCM are likely to be sustained by the tides rather than winds due to (i) the kinetic energy content being dominated by semidiurnal frequencies below the mixed layer (Figure 5d), (ii) there being a spring-neap modulation in the diapycnal diffusivity (Figure 4), and (iii) the summer input of kinetic energy over the entire water column being dominated by the tides rather than the winds (Figures 6d and 6f). Therefore, in summer months, tides are likely to dominate the regional nutrient supply in the North Atlantic subtropical gyre.

4. Basin-Scale Perspectives From a Global Tidal Dissipation Model

The results from our field study reveal the importance of internal tides in driving nutrient fluxes to the DCM over the Mid-Atlantic Ridge. The results imply that in regions of the oligotrophic gyres close to ridges and seamounts, nutrient fluxes are likely to be augmented by internal tides and undergo a fortnightly fluctuation. To test whether the inferences from our field study are significant on larger scales, we employ a tidal model (TPXO8; Egbert & Erofeeva, 2002) and a climatology of nutrient distributions (WOAv2; Garcia et al., 2014) to investigate how variable tidally driven K_z affects the magnitude and distribution of nutrient supply in the subtropics.

The tidal dissipation, D, for the global diffusivity fields was computed using the TPXO8 data set (available from http://volkov.oce.orst.edu/tides/tpxo8_atlas.html), following Egbert and Ray (2001)

$$D = W - \nabla \cdot P, \tag{2}$$

where W is the work done by the tide-generating force and P is the horizontal energy flux vector, which are calculated from

$$W = g\rho \langle \mathrm{U} \cdot \nabla (\eta_{EQ} + \eta_{SAL}) \rangle, \tag{3}$$

$$P = g\rho \langle \mathrm{U}\eta \rangle , \tag{4}$$

where the angular brackets mark time averages over a tidal period, g is gravity, ρ is seawater density, U is the tidal transport vector, η is the tidal amplitude, and η_{sal} and η_{EQ} are the self-attraction and loading amplitude and the equilibrium tide, respectively.

The tidal dissipation energy was then used to compute a vertical diffusivity from a modified version of equation (1)

$$K_z = \Gamma q \frac{D(x,y)F(x,y,z)}{\rho N^2},$$

where q is the dissipation efficiency (the fraction of converted energy that dissipates within the local water column) and F is a function that describes the vertical distribution of the converted energy. The dissipation efficiency, q, is assumed following Vic et al. (2019) to be $q = 0.8$ in the Atlantic and 0.5 in the Pacific; in practice, similar vertical diffusivity profiles are obtained in a sensitivity test using $q = 0.3$ and adding a small constant vertical diffusivity. For the vertical distribution of the converted energy, following St Laurent and Garrett (2002), Schmittner and Egbert (2014) and Melet et al. (2013), we divide the energy in half and assume that one half experiences bottom-enhanced dissipation and the other half is dissipated at a rate proportional to N^2. The bottom intensified half of the energy decays vertically with an e-folding scale of 500 m and thus provides only a small amount to the diffusivity at 500 m (St Laurent & Garrett, 2002). The other half of the local energy dissipation scales proportionally with N^2, such that $F(x,y,z) = N^2(x,y,z)/ \int N^2(x,y,z)dz$, integrated from the surface to the seafloor (e.g., Gregg, 1989; Kunze, 2017). These assumptions for the energy
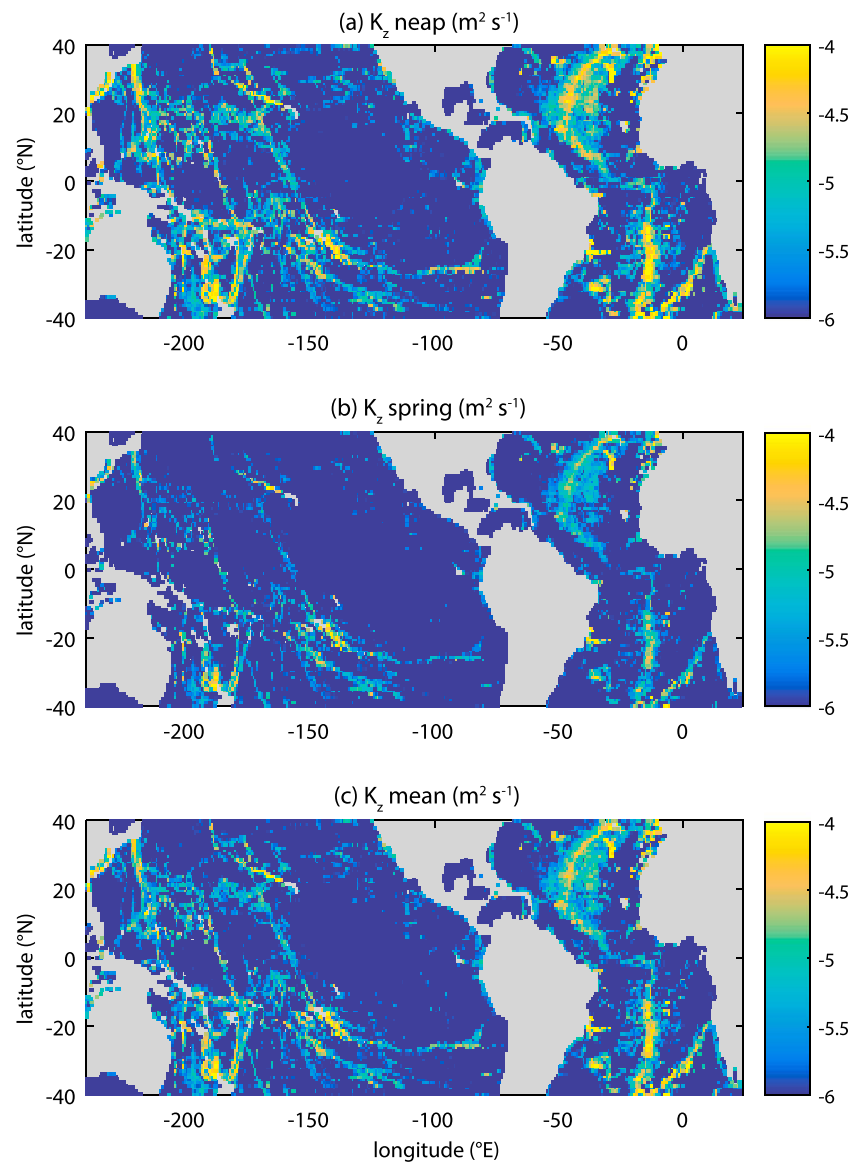
Figure 7. Spring and neap tidal variations in upper ocean diapycnal diffusivity K_z (100–500 m). Upper ocean K_z ($\log_{10}$ m^2/s) is calculated at spring and neap tides over the low-latitude ocean, (a) K_z over neap tides, (b) K_z over spring tides, and (c) tidally averaged K_z.

dissipation lead to dissipation occurring within the thermocline and near the bed, consistent with our observations.

Tidal dissipation estimates over spring and neap tides are used to calculate the fortnightly variation in vertically integrated tidal dissipation. The associated vertical diffusivity is computed by distributing the dissipated energy over depth assuming that the vertical distribution of dissipation is proportional to the squared buoyancy frequency and the local breaking of internal tides. We estimate an upper-ocean diapycnal diffusivity K_z over the Atlantic and Pacific subtropical gyres (100–500 m) associated with internal tide generation ($K_{z\text{-tide}}$), which is in accord with the diffusivity profiles measured from the Mid-Atlantic Ridge field study (Figure 7).

The diapycnal diffusivity estimated from the internal tide $K_{z\text{-tide}}$ is typically 4 times larger over ridges and seamounts compared to over the smooth, deep basins (ridges = <4,000 m, deep basins = >4,000 m). The effects of neap and spring tides are evident, with the area averages fluctuating by more than a factor of 2
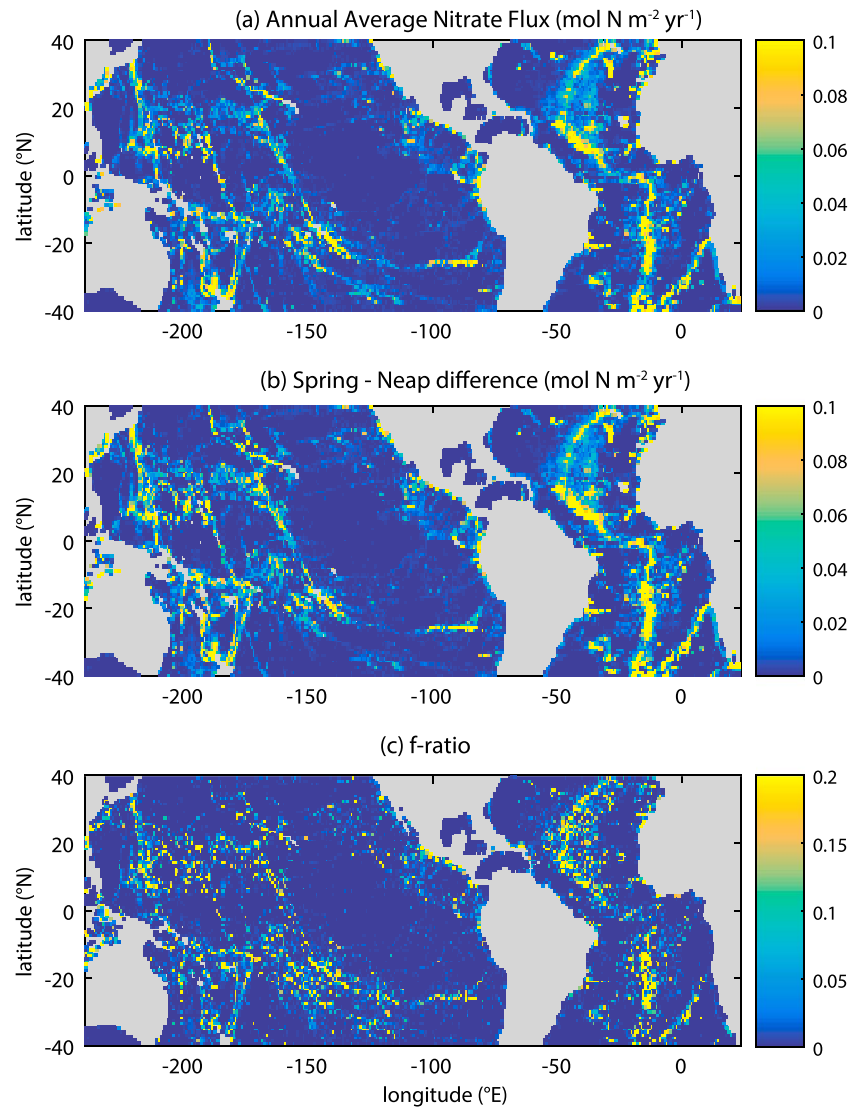
Figure 8. Estimated tidal variation in diapycnal nitrate fluxes over the Atlantic and Pacific basins between 40°S and 40°N. Nutrient gradients were estimated using the maximum gradient in the upper 500 m from WOA climatology. Diapycnal diffusivity was calculated using dissipation from the TPOX8 database assuming that the energy redistributed in the vertical is directly proportional to the buoyancy frequency. (a) Annual average diapycnal nitrate flux in mole of nitrogen per square meter per year. (b) Tidal variability (spring tide minus neap tide) in mole of nitrogen per square meter per year. (c) Estimated f-ratio at the deep chlorophyll maximum. Calculated by assuming that the nitrate flux is converted to carbon fixation following Redfield stoichiometry (C:N = 106:16) and the calculated f-ratio = [Redfield C fixed by internal tidal supply of N] / [annual net primary production from satellite]; annual net primary production is calculated using published methods (Behrenfeld et al., 2006).

over a fortnightly cycle. The tidally generated diapycnal nitrate fluxes are estimated by combining this diapycnal diffusivity $K_{z\text{-tide}}$ with the maximum vertical nitrate gradient in the upper 500 m of each grid using data from WOA13v2 (Figure 8a).

Over large swathes of the subtropical gyres where the influence of tidal-driven mixing is negligible, diapycnal nitrate fluxes are very low (0.01 ± 0.001 mol N·m^{-2}·year^{-1}). In contrast, over regions of ridge systems, area-averaged annual diapycnal nitrate fluxes are 0.05 ± 0.01 mol N·m^{-2}·year^{-1}. Area-integrated fluxes over ridges and the deep ocean reveal that ridge systems which account for only 29% of the study region provide 62% of the tidally generated nitrate flux.

Basin-wide diapycnal nitrate flux estimates over the Atlantic Ocean from internal tides are ~0.03 mol N·m^{-2}·year^{-1}, accounting for approximately one half of current total estimates of diffusive supply from inertial shear and internal tides (~0.05 mol N·m^{-2}·year^{-1}; Williams & Follows, 2011). The diapycnal nitrate fluxes generated by internal tides also importantly create a fortnightly fluctuation in nutrient supply over ridge and seamount regions. The tidal variability in the Atlantic and Pacific subtropical gyres suggests that basin scale-averaged diapycnal nitrate fluxes during spring tides are typically 2–3 times greater than during neap tides.

5. 5. Wider Implications for the Subtropical Gyres

The role of the internal tide in providing enhanced mixing and diapycnal nitrate fluxes to the surface ocean is now discussed in terms of the possible effect on export production and community structure. Over annual or longer timescales, nutrient supply and export production are expected to balance. Thus, estimates of export production in the subtropical ocean require a nitrogen supply term of approximately 0.5–0.9 mol·N·m^{-2}·year^{-1} (Jenkins, 1982; Jenkins & Doney, 2003). This is validated by geochemical estimates of the physical supply of nitrate to the euphotic zone of the subtropical North Atlantic which range between 0.7 and 0.8 mol N·m^{-2}·year^{-1} (Jenkins & Doney, 2003; Stanley et al., 2015). These estimates exclude the biological sources of nitrogen from nitrogen fixation or zooplankton migration which would increase the supply term further (Bianchi et al., 2013; Mahaffey et al., 2005; Tuerena et al., 2015).

Current estimates of spatially averaged diapycnal nitrate supply to the gyres range from 0.002 to 0.055 mol N·m^{-2}·year^{-1} (Lewis et al., 1986, Dietze et al., 2004, Fernández-Castro et al., 2015, Mourino-Carballido et al., 2011; Painter et al., 2013) and thus only provide up to 5–10% of the necessary nitrogen. The remaining required nitrogen may be supplied from a variety of mechanisms (Williams & Follows, 2011): from (i) the atmosphere, via surface deposition or nitrogen fixation (Gruber & Sarmiento, 1997); (ii) a vertical redistribution of nutrients by convection (Williams et al., 2000), additional diapycnal mixing from salt fingering (Oschlies et al., 2003), and mesoscale eddy upwelling (McGillicuddy et al., 1998; Oschlies, 2002); and (iii) a horizontal redistribution of nutrients by horizontal Ekman transfer (Palter et al., 2005; Williams & Follows, 1998), transfer of dissolved organic nitrogen (Roussenov et al., 2006; Williams et al., 2011), and horizontal eddy transfer of nutrients (Lee & Williams, 2000).

The results from this study provide an updated perspective on the diapycnal nutrient supply within the subtropical ocean. The general view is that winds are the primary factor determining nutrient fluxes in the upper ocean. There is a low impact of wind-induced mixing in the central parts of the subtropical gyres, leading to a low diapycnal nutrient supply. Local wind and buoyancy forcing in the subtropics create an environment where there is convection and entrainment in winter and stratification and nutrient limitation in summer. In contrast, tidally induced mixing increases over ridges and seamounts and is not expected to be affected by seasons but instead is modulated on a fortnightly cycle with the spring and neap tides.

These findings suggest a previously overlooked significance for the DCM over the stratified ocean. This ubiquitous layer is generally viewed in the open ocean as a result of local photoacclimation, with increases in biomass occurring only when the layer is influenced by diapycnal mixing acting on the vertical nutrient gradients (Mignot et al., 2014). Interception of the enhanced nitrate flux by phytoplankton within the DCM will lead to changes that are not detected in satellite estimates (Letelier et al., 2004). The internal tidal waves may also boost light availability for DCM phytoplankton (Evans et al., 2008). The enhanced mixing will transfer nutrients upward in the DCM to regions of more light. At the same time the waves will oscillate the DCM through the light gradient, as seen in the excursions of isotherms at the mooring site (Figure S3). In our study, isopycnals in the base of the DCM over the ridge were seen to be oscillated about their mean depth by $\pm$10 m at neap tides and $\pm$20 m at spring tides. Thus, predictable fortnightly and semidiurnal tidal oscillations vary the light and nutrient availability over ridges, creating a changing biome.

The ecosystem implications of the tidal mixing are now considered. The upper euphotic layer in the subtropical ocean is dominated by small-celled cyanobacteria (Legendre & Rivkin, 2002). In contrast the species assemblage at the DCM is determined by the ambient nutrient and light availability (Sharples et al., 2007) and in the subtropics contains a diverse assemblage of prokaryote and eukaryote phytoplankton (McManus & Dawson, 1994). Hot spots of tidally induced mixing increase the proportion of new nitrate

supply to the DCM which may shift local community *f*-ratios (the ratio of primary production fueled by nitrate compared to regenerated nitrogen; Fawcett et al., 2011).

We explored these potential changes by assuming that tidal nitrate fluxes over the oligotrophic gyres are converted to carbon following Redfield stoichiometry (C:N = 106:16). The carbon fixation thus provides an estimate for new production (as supplied from the thermocline). The community *f*-ratio is calculated using satellite-based estimates of primary production (Behrenfeld et al., 2006; Behrenfeld & Falkowski, 1997), whereby, the community *f*-ratio is equal to [Redfield carbon fixed by internal tidal supply of nitrogen] / [annual net primary production from satellite]. Estimated *f*-ratios are enhanced over ridges and seamounts across the wider subtropical ocean (Figure 8c).

The differing nitrogen uptake strategies of phytoplankton will alter the success of particular species or algal groups depending on the availability of recycled ammonium or nitrate from the underlying thermocline. For example, eukaryotes are adapted to assimilate new nitrate over ammonium in subtropical regions (Fawcett et al., 2011). In areas of low diapycnal mixing, the available fixed nitrogen is likely to be dominated by recycled nitrogen, where prokaryotes can outcompete eukaryotes for the less energy expensive source of nitrogen (Sharples et al., 2009).

Reducing nutrient and light limitation can further increase growth rates and/or shift the community size structure toward larger species such as diatoms, increasing the potential for carbon export (Maranon, 2015; Siegel et al., 2014). Thus, modulating light and nutrient conditions at the DCM over ridges and seamounts could have important consequences for local community structure, which may have implications for particulate carbon export (Boyd & Trull, 2007) and enhance pelagic biodiversity up into higher trophic levels (Morato et al., 2010).

6. Conclusions

This study explores the implications of tidally generated diapycnal nutrient fluxes in the vast subtropical ocean gyres, where diapycnal mixing is often considered to be dominated by the wind and is relatively weak over the central parts of these gyres. Our field campaign in the North Atlantic subtropical gyre reveals that there is enhanced tidal dissipation and diapycnal mixing along the Mid-Atlantic Ridge, which extends over much of the water column. This enhanced mixing redistributes nutrients from the thermocline to the surface ocean and provides an increased diapycnal flux of nutrients to the DCM. Our analyses from the field study reveal that these enhanced nutrient fluxes also have a predictable fortnightly variability, with an eightfold increase in nitrate supply to the DCM. This enhanced mixing from the tides crucially acts over a depth range where there are available nutrients and so sustaining phytoplankton growth in the DCM. In contrast, the mixing from winds is strongest within the surface mixed layer where there are a lack of nutrients over much of the year.

Upscaling our fieldwork by using a global tidal dissipation database, we find that this spring-neap enhancement in diapycnal nitrate fluxes is ubiquitous over regions of rough or steep sloping topography. This mechanism of tidally enhanced mixing in sustaining nutrient supply to the upper ocean is important on a global scale where there is shallow topography, including ridges and sea mounts. This enhanced diapycnal supply of nutrients over shallow topography is expected to help sustain export production and modify the local community structure, as well as potentially affect the ecosystem response to future ocean warming scenarios.

References

Alford, M. (2003). Redistribution of energy available for ocean mixing by long-range propagation of internal waves. *Nature*, *423*(6936), 159–162. https://doi.org/10.1038/nature01628

Alford, M. H., Cronin, M. F., & Klymak, J. M. (2012). Annual cycle and depth penetration of wind-generated near-inertial internal waves at Ocean Station Papa in the Northeast Pacific. *Journal of Physical Oceanography*, *42*(6), 889–909. https://doi.org/10.1175/JPO-D-11-092.1

Alford, M. H., MacKinnon, J. A., Simmons, H. L., & Nash, J. D (2016). Near-Inertial Internal Gravity Waves in the Ocean. In C. A. Carlson& S. J. Giovannoni (Eds.), *Annual Review of Marine Science* (Vol. 8, pp. 95–123).

Behrenfeld, M. J., & Falkowski, P. G. (1997). Photosynthetic rates derived from satellite-based chlorophyll concentration. *Limnology and Oceanography*, *42*(1), 1–20. https://doi.org/10.4319/lo.1997.42.1.0001

Behrenfeld, M. J., O'Malley, R. T., Siegel, D. A., McClain, C. R., Sarmiento, J. L., Feldman, G. C., et al. (2006). Climate-driven trends in contemporary ocean productivity. *Nature*, *444*(7120), 752–755. https://doi.org/10.1038/nature05317

Bianchi, D., Stock, C., Galbraith, E. D., & Sarmiento, J. L. (2013). Diel vertical migration: Ecological controls and impacts on the biological pump in a one-dimensional ocean model. *Global Biogeochemical Cycles*, *27*, 478–491. https://doi.org/10.1002/gbc.20031

Boyd, P. W., & Trull, T. W. (2007). Understanding the export of biogenic particles in oceanic waters: Is there consensus? *Progress in Oceanography*, *72*(4), 276–312. https://doi.org/10.1016/j.pocean.2006.10.007

Cuypers, Y., Bouruet-Aubertot, P., Vialard, J., & Mcphaden, M. J. (2017). Focusing of internal tides by near-inertial waves. *Geophysical Research Letters*, *44*, 2398–2406. https://doi.org/10.1002/2017GL072625

Dietze, H., Oschlies, A., & Kahler, P. (2004). Internal-wave-induced and double-diffusive nutrient fluxes to the nutrient-consuming surface layer in the oligotrophic subtropical North Atlantic. *Ocean Dynamics*, *54*(1), 1–7. https://doi.org/10.1007/s10236-003-0060-9

Egbert, G. D., & Erofeeva, S. Y. (2002). Efficient inverse modeling of barotropic ocean tides. *Journal of Atmospheric and Oceanic Technology*, *19*(2), 183–204. https://doi.org/10.1175/1520-0426(2002)019<0183:EIMOBO>2.0.CO;2

Egbert, G. D., & Ray, R. D. (2000). Significant dissipation of tidal energy in the deep ocean inferred from satellite altimeter data. *Nature*, *405*(6788), 775–778. https://doi.org/10.1038/35015531

Egbert, G. D., & Ray, R. D. (2001). Estimates of M-2 tidal energy dissipation from TOPEX/Poseidon altimeter data. *Journal of Geophysical Research*, *106*(C10), 22,475–22,502. https://doi.org/10.1029/2000JC000699

Evans, M. A., MacIntyre, S., & Kling, G. W. (2008). Internal wave effects on photosynthesis: Experiments, theory, and modeling. *Limnology and Oceanography*, *53*(1), 339–353. https://doi.org/10.4319/lo.2008.53.1.0339

Falahat, S., Nycander, J., Roquet, F., Thurnherr, A. M., & Hibiya, T. (2014). Comparison of calculated energy flux of internal tides with microstructure measurements. *Tellus Series A-Dynamic Meteorology and Oceanography*, *66*(1). https://doi.org/10.3402/tellusa.v66.23240

Fawcett, S. E., Lomas, M., Casey, J. R., Ward, B. B., & Sigman, D. M. (2011). Assimilation of upwelled nitrate by small eukaryotes in the Sargasso Sea. *Nature Geoscience*, *4*(10), 717–722. https://doi.org/10.1038/ngeo1265

Fernández-Castro, B., Mouriño-Carballido, B., Marañón, E., Chouciño, P., Gago, J., Ramírez, T., et al. (2015). Importance of salt fingering for new nitrogen supply in the oligotrophic ocean. *Nature Communications*, *6*(1), 8002. https://doi.org/10.1038/ncomms9002

Garcia, H. E., Locarnini, R. A., Boyer, T. P., Antonov, J. I., Baranova, O. K., Zweng, M. M., et al. (2014). *World Ocean Atlas 2013, Volume 4: Dissolved Inorganic Nutrients (phosphate, nitrate, silicate)*. In S. Levitus (Ed.), A. Mishonov Technical (Ed.). *NOAAtlas NESDIS 76* (pp. 25).

Garrett, C., & Kunze, E. (2007). Internal tide generation in the deep ocean. *Annual Review of Fluid Mechanics*, *39*(1), 57–87. https://doi.org/10.1146/annurev.fluid.39.050905.110227

Gregg, M. C. (1989). Scaling turbulent dissipation in the thermocline. *Journal of Geophysical Research*, *94*(C7), 9686–9698. https://doi.org/10.1029/JC094iC07p09686

Gregg, M. C., D'Asaro, E. A., Riley, J. J., & Kunze, E. (2018). Mixing efficiency in the ocean. *Annual Review of Marine Science*, *10*(1), 443–473. https://doi.org/10.1146/annurev-marine-121916-063643

Gruber, N., & Sarmiento, J. L. (1997). Global patterns of marine nitrogen fixation and denitrification. *Global Biogeochemical Cycles*, *11*(2), 235–266. https://doi.org/10.1029/97GB00077

Hibiya, T., & Nagasawa, M. (2004). Latitudinal dependence of diapycnal diffusivity in the thermocline estimated using a finescale parameterization. *Geophysical Research Letters*, *31*, L01301. https://doi.org/10.1029/2003GL017998

Jenkins, W. J. (1982). Oxygen utilization rates in the North-Atlantic sub-tropical gyre and primary production in oligotrophic systems. *Nature*, *300*(5889), 246–248. https://doi.org/10.1038/300246a0

Jenkins, W. J., & Doney, S. C. (2003). The subtropical nutrient spiral. *Global Biogeochemical Cycles*, *17*(4), 1110. https://doi.org/10.1029/2003GB002085

Kunze, E. (2017). Internal-wave-driven mixing: Global geography and budgets. *Journal of Physical Oceanography*, *47*(6), 1325–1345. https://doi.org/10.1175/JPO-D-16-0141.1

Kunze, E., Firing, E., Hummon, J. M., Chereskin, T. K., & Thurnherr, A. M. (2006). Global abyssal mixing inferred from lowered ADCP shear and CTD strain profiles. *Journal of Physical Oceanography*, *36*(8), 1553–1576. https://doi.org/10.1175/JPO2926.1

Lavergne, C., Falhat, S., Madec, G., Roquet, F., Nycander, J., & Vic, C. (2019). Toward global maps of internal tide energy sinks. *Ocean Modelling*, *137*, 52–75. https://doi.org/10.1016/j.ocemod.2019.03.010

Lee, M. M., & Williams, R. G. (2000). The role of eddies in the isopycnic transfer of nutrients and their impact on biological production. *Journal of Marine Research*, *58*(6), 895–917. https://doi.org/10.1357/002224000763485746

Lefauve, A., Muller, C., & Melet, A. (2015). A three-dimensional map of tidal dissipation over abyssal hills. *Journal of Geophysical Research: Oceans*, *120*, 4760–4777. https://doi.org/10.1002/2014JC010598

Legendre, L., & Rivkin, R. B. (2002). Fluxes of carbon in the upper ocean: Regulation by food-web control nodes. *Marine Ecology Progress Series*, *242*, 95–109. https://doi.org/10.3354/meps242095

Letelier, R. M., Karl, D. M., Abbott, M. R., & Bidigare, R. R. (2004). Light driven seasonal patterns of chlorophyll and nitrate in the lower euphotic zone of the North Pacific Subtropical Gyre. *Limnology and Oceanography*, *49*(2), 508–519. https://doi.org/10.4319/lo.2004.49.2.0508

Lewis, M. R., Harrison, W. G., Oakey, N. S., Hebert, D., & Platt, T. (1986). Vertical nitrate fluxes in the oligotrophic ocean. *Science*, *234*(4778), 870–873. https://doi.org/10.1126/science.234.4778.870

MacKinnon, J. A., Zhao, Z., Whalen, C. B., Waterhouse, A. F., Trossman, D. S., Sun, O. M., et al. (2017). Climate process team on internal wave-driven ocean mixing. *Bulletin of the American Meteorological Society*, *98*(11), 2429–2454. https://doi.org/10.1175/BAMS-D-16-0030.1

Mahaffey, C., Michaels, A. F., & Capone, D. G. (2005). The conundrum of marine N-2 fixation. *American Journal of Science*, *305*(6-8), 546–595. https://doi.org/10.2475/ajs.305.6-8.546

Maranon, E. (2015). Cell Size as a Key Determinant of phytoplankton metabolism and community structure. *Annual Review of Marine Science*, *7*(1), 241–264. https://doi.org/10.1146/annurev-marine-010814-015955

McGillicuddy, D. J., Robinson, A. R., Siegel, D. A., Jannasch, H. W., Johnson, R., & Dickeys, T. (1998). Influence of mesoscale eddies on new production in the Sargasso Sea. *Nature*, *394*(6690), 263–266. https://doi.org/10.1038/28367

McManus, G. B., & Dawson, R. (1994). Phytoplankton pigments in the deep chlorophyll maximum of the Caribbean Sea and the western tropical Atlantic Ocean. *Marine Ecology Progress Series*, *113*(1-2), 199–206. https://doi.org/10.3354/meps113199

Melet, A., Legg, S., & Hallberg, R. (2016). Climatic impacts of parameterized local and remote tidal mixing. *Journal of Climate*, *29*(10), 3473–3500. https://doi.org/10.1175/JCLI-D-15-0153.1

Melet, A., Hallberg, R., Legg, S., & Polzin, K. (2013). Sensitivity of the ocean state to the vertical distribution of internal-tide-driven mixing. *Journal of Physical Oceanography*, *43*(3), 602–615. https://doi.org/10.1175/jpo-d-12-055.1

Mignot, A., Claustre, H., Uitz, J., Poteau, A., D'Ortenzio, F., & Xing, X. G. (2014). Understanding the seasonal dynamics of phytoplankton biomass and the deep chlorophyll maximum in oligotrophic environments: A Bio-Argo float investigation. *Global Biogeochemical Cycles*, *28*, 856–876. https://doi.org/10.1002/2013GB004781

Morato, T., Hoyle, S. D., Allain, V., & Nicol, S. J. (2010). Seamounts are hotspots of pelagic biodiversity in the open ocean. *Proceedings of the National Academy ofSciences of the United States of America*, *107*(21), 9707–9711. https://doi.org/10.1073/pnas.0910290107

Mouriño-Carballido, B., Graña, R, Fernàndez, A., Bode, A., Varela, M., Domínguez, J. F, & Marañón, E. (2011). Importance of N2fixation vs. nitrate eddy diffusion along a latitudinal transect in the Atlantic Ocean. *Limnology and Oceanography*, *56*(3), 999–1007. https://doi.org/10.4319/lo.2011.56.3.0999

Munk, W., & Wunsch, C. (1998). Abyssal recipes II: Energetics of tidal and wind mixing. *Deep-Sea Research Part I-Oceanographic Research Papers*, *45*(12), 1977–2010. https://doi.org/10.1016/S0967-0637(98)00070-3

Oakey, N. S. (1982). Determination of the rate of dissipation of turbulent energy from simultaneous temperature and velocity shear microstructure measurements. *Journal of Physical Oceanography*, *12*(3), 256–271. https://doi.org/10.1175/1520-0485(1982)012<0256: DOTROD>2.0.CO;2

Omand, M. M., & Mahadevan, A. (2015). The shape of the oceanic nitracline. *Biogeosciences*, *12*(11), 3273–3287. https://doi.org/10.5194/bg-12-3273-2015

Osborn, T. (1980). Estimates of the local rate of vertical diffusion from dissipation measurements. *Journal of Physical Oceanography*, *10*(1), 83–89. https://doi.org/10.1175/1520-0485(1980)010<0083:EOTLRO>2.0.CO;2

Oschlies, A. (2002). Nutrient supply to the surface waters of the North Atlantic: A model study. *Journal of Geophysical Research*, *107*(C5), 3046. https://doi.org/10.1029/2000JC000275

Oschlies, A., Dietze, H., & Kahler, P. (2003). Salt-finger driven enhancement of upper ocean nutrient supply. *Geophysical Research Letters*, *30*(23), 2204. https://doi.org/10.1029/2003GL018552

Painter, S. C., Patey, M. D., Forryan, M. D., & Torres-Valdes, S. (2013). Evaluating the balance between vertical diffusive nitrate supply and nitrogen fixation with reference to nitrate uptake in the eastern subtropical North Atlantic Ocean. *Journal of Geophysical Research: Oceans*, *118*, 5732–5749. https://doi.org/10.1002/jgrc.20416

Palter, J. B., Lozier, M. S., & Barber, R. T. (2005). The effect of advection on the nutrient reseervoir in the North Atlantic subtropical gyre. *Nature*, *437*(7059), 687–692. https://doi.org/10.1038/nature03969

Pelegri, J. L., Marrero-Diaz, A., & Ratsimandresy, A. W. (2006). Nutrient irrigation of the North Atlantic. *Progress in Oceanography*, *70*(2-4), 366–406. https://doi.org/10.1016/j.pocean.2006.03.018

Polzin, K. L., Toole, J. M., Ledwell, J. R., & Schmitt, R. W. (1997). Spatial variability of turbulent mixing in the abyssal ocean. *Science*, *276*(5309), 93–96. https://doi.org/10.1126/science.276.5309.93

Rippeth, T. P., & Inall, M. E. (2002). Observations of the internal tide and associated mixing across the Malin Shelf. *Journal of Geophysical Research*, *107*(C4), 3028. https://doi.org/10.1029/2000JC000761

Roussenov, V., Williams, R. G., Mahaffey, C., & Wolff, G. A. (2006). Does the transport of dissolved organic nutrients affect export production in the Atlantic Ocean? *Global Biogeochemical Cycles*, *20*, GB3002. https://doi.org/10.1029/2005GB002510

Sarmiento, J. L., Gruber, N., Brzezinski, M. A., & Dunne, J. P. (2004). High-latitude controls of thermocline nutrients and low latitude biological productivity. *Nature*, *427*(6969), 56–60. https://doi.org/10.1038/nature02127

Schmittner, A., & Egbert, G. D. (2014). An improved parameterization of tidal mixing for ocean models. *Geoscientific Model Development*, *7*(1), 211–224. https://doi.org/10.5194/gmd-7-211-2014

Sharples, J., Moore, C. M., Hickman, A. E., Holligan, P. M., Tweddle, J. F., Palmer, M. R., & Simpson, J. H. (2009). Internal tidal mixing as a control on continental margin ecosystems. *Geophysical Research Letters*, *36*, L23603. https://doi.org/10.1029/2009GL040683

Sharples, J., Tweddle, J. F., Mattias Green, J. A., Palmer, M. R., Kim, Y. N., Hickman, A. E., et al. (2007). Spring-neap modulation of internal tide mixing and vertical nitrate fluxes at a shelf edge in summer. *Limnology and Oceanography*, *52*(5), 1735–1747. https://doi.org/10.4319/lo.2007.52.5.1735

Siegel, D. A., Buesseler, K. O., Doney, S. C., Sailley, S. F., Behrenfeld, M. J., & Boyd, P. W. (2014). Global assessment of ocean carbon export by combining satellite observations and food-web models. *Global Biogeochemical Cycles*, *28*, 181–196. https://doi.org/10.1002/2013GB004743

St Laurent, L., & Garrett, C. (2002). The role of internal tides in mixing the deep ocean. *Journal of Physical Oceanography*, *32*(10), 2882–2899. https://doi.org/10.1175/1520-0485(2002)032<2882:TROITI>2.0.CO;2

Stanley, R. H. R., Jenkins, W. J., Doney, S. C., & Lott, D. E. (2015). The He-3 flux gauge in the Sargasso Sea: A determination of physical nutrient fluxes to the euphotic zone at the Bermuda Atlantic Time-series Site. *Biogeosciences*, *12*(17), 5199–5210. https://doi.org/10.5194/bg-12-5199-2015

Toole, J. M. (2007). Temporal characteristics of abyssal finescale motions above rough bathymetry. *Journal of Physical Oceanography*, *37*(3), 409–427. https://doi.org/10.1175/JPO2988.1

Tuerena, R. E., Ganeshram, R. S., Geibert, W., Fallick, A. E., Dougans, J., Tait, A., et al. (2015). Nutrient cycling in the Atlantic basin: The evolution of nitrate isotope signatures in water masses. *Global Biogeochemical Cycles*, *29*, 1830–1844. https://doi.org/10.1002/2015GB005164

Tweddle, J. F., Sharples, J., Palmer, M. R., Davidson, K., & McNeill, S. (2013). Enhanced nutrient fluxes at the shelf sea seasonal thermocline caused by stratified flow over a bank. *Progress in Oceanography*, *117*, 37–47. https://doi.org/10.1016/j.pocean.2013.06.018

Vic, C., Naveira Garabato, A. C., Green, J. A. M., Spingys, C., Forryan, A., Zhao, Z., & Sharples, J. (2018). The lifecycle of semidiurnal internal tides over the northern Mid-Atlantic Ridge. *Journal of Physical Oceanography*, *48*(1), 61–80. https://doi.org/10.1175/JPO-D-17-0121.1

Vic, C., Naveira Garabato, A. C., Green, J. A. M., Waterhouse, A. F., Zhao, Z., Melet, A., et al. (2019). Deep-ocean mixing driven by small-scale internal tides. *Nature Communications*, *10*(1), 2099. https://doi.org/10.1038/s41467-019-10149-5

Villamaña, M., Mouriño-Carballido, B., Marañón, E., Cermeño, P., Chouciño, P., da Silva, J. C. B., et al. (2017). Role of internal waves on mixing, nutrient supply and phytoplankton community structure during spring and neap tides in the upwelling ecosystem of Ría de Vigo (NW Iberian Peninsula). *Limnology and Oceanography*, *62*(3), 1014–1030. https://doi.org/10.1002/lno.10482

Waterhouse, A. F., MacKinnon, J. A., Nash, J. D., Alford, M. H., Kunze, E., Simmons, H. L., et al. (2014). Global patterns of diapycnal mixing from measurements of the turbulent dissipation rate. *Journal of Physical Oceanography*, *44*(7), 1854–1872. https://doi.org/10.1175/JPO-D-13-0104.1

Whalen, C. B., MacKinnon, J. A., & Talley, L. D. (2018). Large-scale impacts of the mesoscale environment on mixing from wind-driven internal waves. *Nature Geoscience*, *11*(11), 842–847. https://doi.org/10.1038/s41561-018-0213-6

Williams, R. G., & Follows, M. J. (1998). The Ekman transfer of nutrients and maintenance of new production over the North Atlantic. *Deep-Sea Research Part I-Oceanographic Research Papers*, *45*(2-3), 461–489. https://doi.org/10.1016/S0967-0637(97)00094-0

Williams, R. G., & Follows, M. J. (2011). *Ocean dynamics and the carbon cycle: Principles and mechanisms*. Cambridge University Press. https://doi.org/10.1017/CBO9780511977817

Williams, R. G., McDonagh, E., Roussenov, V. M., Torres-Valdes, S., King, B., Sanders, R., & Hansell, D. A. (2011). Nutrient streams in the North Atlantic: Advective pathways of inorganic and dissolved organic nutrients. *Global Biogeochemical Cycles*, *25*, GB4008. https://doi.org/10.1029/2010GB003853

Williams, R. G., McLaren, A. J., & Follows, M. J. (2000). Estimating the convective supply of nitrate and implied variability in export production over the North Atlantic. *Global Biogeochemical Cycles*, *14*(4), 1299–1313. https://doi.org/10.1029/2000GB001260